Seasonal variability of salt transport during the Indian Ocean monsoons

Ebenezer S. Nyadjro,[1] Bulusu Subrahmanyam,[1,2] and Jay F. Shriver[3]

Received 24 January 2011; revised 18 May 2011; accepted 31 May 2011; published 27 August 2011.

[1] The seasonal variability of salinity transport in the Indian Ocean is investigated using the high-resolution global HYbrid Coordinate Ocean Model (HYCOM). Mechanisms and physical parameters that control the salinity budget are examined. Results show the influence of freshwater forcing and zonal advection as the dominant mechanisms of sea surface salinity (SSS) variability. Precipitation is highest in the eastern Bay of Bengal (BoB), where it shows seasonal variation, and in the south equatorial eastern Indian Ocean (EIO), where it was consistently high year-round. These patterns result in significant seasonal variation in the SSS in the BoB and almost no variation in the EIO. Zonal SSS transport was higher than meridional SSS transport with the strongest seasonality observed along the Sri Lankan region. Results of depth-integrated transport show northward salt transport in the bottom layers and a southward salt transport in the surface layers. The 4 year mean net flux of depth-integrated salt transport was southward (-154.8×10^6 kg/s to -552.4×10^6 kg/s) at all latitudes except at 20°N, where it was northward (396×10^6 kg/s). Transport generally increases southward with the highest transports occurring in the south (10°S–35°S) and a maximum at 30°S. Analyses of meridional Ekman volume and salt transport show a predominantly southward transport, an indication of the strong influence of SW monsoonal winds. It is anticipated that this study will be useful in computing salt transport using satellite-derived salinity data from the European Space Agency (ESA) Soil Moisture and Ocean Salinity (SMOS) and NASA Aquarius salinity missions.

Citation: Nyadjro, E. S., B. Subrahmanyam, and J. F. Shriver (2011), Seasonal variability of salt transport during the Indian Ocean monsoons, *J. Geophys. Res.*, *116*, C08036, doi:10.1029/2011JC006993.

1. Introduction

[2] The variability and transport of salinity are important in the understanding of the global hydrologic cycle and the earth's climate, as well as oceanic processes such as circulation and heat storage [*Delcroix et al.*, 1996; *Illig and Perigaud*, 2007]. Except on geologic time scales and the consequence of climate change, net ocean salinity does not change. The differences observed are usually the result of the influence of precipitation (P), evaporation (E), river runoff (R), advection and mixing [*Wijffels et al.*, 1992; *Han and McCreary*, 2001; *Prasad and Ikeda*, 2002a]. The magnitudes of E, P and R define the surface freshwater flux of a region and they show significant variability in the Indian Ocean. This is as a result of the seasonal reversal of winds, which causes monsoon cycles to vary greatly thereby affecting the distribution and variability of sea surface salinity (SSS) [*Levitus*, 1988; *Nyadjro et al.*, 2010]. In the determination of the conservation of salt in the surface mixed layer, E and P are important parameters that are incorporated in the mathematical expressions of the salinity budget [*Delcroix and Henin*, 1991; *Foltz and McPhaden*, 2008]. The magnitude of variability in E and P especially, and that of other salinity tendency terms such as mixing, vertical and horizontal diffusions, may, however, not lead to an analogous magnitude in variability of salt transport as the processes affecting the tendency terms vary in time and space [*Dourado and Caniaux*, 2003].

[3] Salinity variability in the Indian Ocean can be influenced by water circulation and ocean-atmosphere coupled interactions such as the Madden-Julian Oscillation (MJO) [*Joseph and Freeland*, 2005]. As a consequence of the differences in E-P and oceanic processes such as advection and vertical mixing, salinity varies among the Indian Ocean basins. Surface salinity is higher in the northwestern end as a result of E exceeding P in the Arabian Sea (AS) and lower in the northeastern end due to higher precipitation in that region, river runoff into the Bay of Bengal (BoB) and low-salinity water from the Indonesian Throughflow (ITF) [*Piola and Gordon*, 1984; *Donguy and Meyers*, 1996; *Joseph and Freeland*, 2005]. For example, the Brahmaputra, Ganga, Irrawaddy, Godavari and Mahanadi rivers, which are among the world's 50 largest rivers, flow into the

[1]Marine Science Program, University of South Carolina, Columbia, South Carolina, USA.
[2]Department of Earth and Ocean Sciences, University of South Carolina, Columbia, South Carolina, USA.
[3]Naval Research Laboratory, Stennis Space Center, Mississippi, USA.

0148-0227/11/2011JC006993

BoB [*Sengupta et al.*, 2006]. It is estimated that 4700 and 3000 km^3/yr of freshwater enters BoB via local precipitation and river discharge respectively; while 3600 km^3/yr is lost via evaporation [*Rajamani et al.*, 2006]. On the whole, the Indian Ocean is considered an evaporative basin as it loses about 1.392×10^4 km^3/yr of freshwater in net evaporation to the atmosphere [*Wijffels et al.*, 1992]. The variation in the flux parameters therefore can set up seasonal differences in the initiation, sustenance and variability of salinity transport in the Indian Ocean especially given the dynamics of processes associated with the monsoons.

[4] Paleoceanographic records have shown that the strength of monsoons varies on several time scales and their effects on oceanographic conditions and processes could as well be varied [*Webster et al.*, 1998; *Murtugudde et al.*, 2007]. Nevertheless, the causes and patterns in salinity distribution and variability are quite consistent. For example, although one of the main indicators of the strength of a monsoon is the magnitude of precipitation (which significantly affects salinity values), *Vinayachandran* [2004] contends that the strength and duration of monsoonal winds were more important for AS cooling (and by inference salinity variation) than the amount of precipitation into the BoB and subsequently into the AS.

[5] In the Indian Ocean, salinity contributes to the formation of the barrier layer as a result of stratification within the isothermal layer, controls vertical mixing, mixed layer and warm pool dynamics [*Han et al.*, 2001; *Durand et al.*, 2007; *Hareesh Kumar et al.*, 2009]. The transport of salt therefore has the potential of affecting these processes. Additionally, it is important in the understanding of the global water budget which is one of the main forcing mechanisms of the thermohaline circulation. Increase in surface salinity when aided by deep convection could lead to the formation of deep water masses. This phenomenon has the potential of inducing a meridional density gradient that affects meridional circulation and aids the transport of salt [*Sévellec et al.*, 2008; *Czaja*, 2009]. Deep convection could be inhibited by the freshening of the surface waters. To sustain deep convection and meridional circulation, ocean currents transport salt to balance out the freshening [*Oka and Hasumi*, 2006].

[6] Surface circulation in the Indian Ocean undergoes seasonal variability as a result of reversal of winds, the effects of which is well noticeable in the northern part of the ocean. The Southwest (SW) monsoon occurs between June and September while the Northeast monsoon (NE) occurs between November and February. The onset of the SW monsoon is usually characterized by weak alongshore winds off the coast of Somalia. It then matures in June and peaks in the later parts of July [*Webster et al.*, 1999]. During the SW monsoon, the highly saline Arabian Sea Water mass (ASW), which occurs at a depth of about 0–100 m, spreads with the eastward flowing SW Monsoon Current (SMC) carrying salty water into the BoB [*Morrison*, 1997; *Schott and McCreary*, 2001]. The Somali Current also flows northward into the AS. During this season too, the humid southwesterly winds from the oceans causes increased surface cooling and significant upwelling along the coasts of the Arabian Seas [*Murtugudde et al.*, 2007]. This is capable of bringing high saline waters to the sea surface and coupled with high evaporation, makes SSS in this region usually higher than other times of the year [*Prasad and Ikeda*, 2002b]. The NE monsoon is characterized by dry and weak northwesterly winds from Asian landmass. In response to the reversed winds, the Somali current also reverses and flows southwards. During this season, less saline waters from the BoB is carried by the southward flowing East India Coastal Current (EICC) into the West India Coastal Current (WICC) [*Vinayachandran et al.*, 1999; *Prasanna Kumar et al.*, 2004]. The westward flowing Northeast Monsoon Current (NMC) also brings less saline water into the WICC which then flows northward along the west coast of India into the AS [*Schott and McCreary*, 2001; *Subrahmanyam et al.*, 2011]. This, however, does not result in drastic drop in AS SSS as the passage of the dry NE winds results in evaporative cooling, which ensures a high salinity [*Prasad and Ikeda*, 2002a].

[7] The water circulation in the southern Indian Ocean is predominantly a consequence of a wind stress curl forced subtropical gyre that occurs in the upper 1000 m and made up of the Agulhas Current, East Madagascar Current (EMC), Mozambique Current (MC) and the South Equatorial Current (SEC). The net flow of these is southward and dominated by the Agulhas Current [*Gordon et al.*, 1992]. The flows in the deep and abyssal sections of the region are dominated by the presence of bottom currents that transport the Circumpolar Deep Water (CDW, occurring at ~2000–3000 m) and the Antarctic Bottom Water (AABW, occurring below ~3800 m) northward [*Fu*, 1986]. The CDW enters the southwestern end of the Indian Ocean through the Agulhas Basin then into the Mozambique Basin, its northernmost extent is, however, believed to be Davie Ridge (~2.5 km high) in the Mozambique Channel [*Toole and Warren*, 1993; *Mantyla and Reid*, 1995]. Later studies by *van Aken et al.* [2004], however, suggest that about 2 Sv of the top half of the NADW flow across the Ridge into the Somali Basin. This water travels further north into the Arabian Basin, where it gradually upwells into and becomes part of the overlying Indian Deep Water (IDW). The flow of this water is predominantly northward and its influence causes northward salt and volume fluxes. This water which typically occurs between 1500 to 3800 m also accounts for the northward flux of waters in the intermediate-deep layers. In the Arabian Basin, high-saline Red Sea and Persian Gulf waters vertically mix with the underlying waters thereby increasing the salinity of the deeper waters [*Piola and Gordon*, 1984]. The Red Seawater has been reported to have been seen as far south as the southern end of the Mozambique Channel [*Gründlingh*, 1985].

[8] Due to the limitation of salinity observations, basin scale studies of salinity transport have been a challenge in the Indian Ocean. Many such studies have relied heavily on numerical simulations, which sometimes suffer especially from the estimation of freshwater flux terms [*Murtugudde and Busalacchi*, 1998]. This has been explained as arising from the fact that the spatial distribution of atmospheric input functions is non-Gaussian [*Tomczak*, 1995; *Dourado and Caniaux*, 2003]. Other challenges have been the poor representation of coastal currents and the dominance of Ekman drift over geostrophy in the western coast of India that leads to differences between observed and modeled SSS [*Prasad and Ikeda*, 2002b]. Using passive tracers to map the exchange of salt in a multilayer upper ocean model, *Jensen*

[2001] attributed the southward advection of low-saline water from the BoB to Ekman drift. His model, however, did not find a significant transport of water from the BoB into the AS although *Esenkov et al.* [2003] did. *Esenkov et al.*'s [2003] Miami Isopycnic Coordinate Ocean Model (MICOM) could not capture the influence of the pathway between Sri Lanka and India, known as the Palk Strait, in the exchange of salt between AS and BoB as this was closed in the model. In our HYCOM simulations, the Palk Strait was opened and allows water exchange between the BoB and the Gulf of Mannar.

[9] The bulk of the Indian Ocean lies in the Southern hemisphere for which data is very sparse. In spite of its role in global climate phenomena, the Indian Ocean is poorly sampled and not many salt transport estimates exist for it. The few studies available are limited to a small number of sections (typically one or two latitudinal bands) thereby making the basin-wide understanding of processes quite a challenge. To the best of our knowledge therefore, this is the first basin-scale depth-integrated salt transport study for the Indian Ocean. It hopes to build on earlier works by using a 1/12° high-resolution HYbrid Coordinate Ocean Model (HYCOM) simulation during 2003–2006 to study salt transport in the Indian Ocean. It describes the seasonal variability of salinity and the relative importance of flux terms in the advection process. It also investigates the pathways of salt exchange as a function of depth in the Indian Ocean. The complex topography of the Indian Ocean offers bathymetric constraints for which the approach used in the study does not clearly highlight the role of depth features such as sills in the transport; nevertheless, a general pattern of the salt transport is achieved.

2. Model, Data, and Methods

2.1. HYCOM Simulations

[10] The model used in this study is global HYCOM, which was developed from the Miami Isopycnic Coordinate Ocean Model (MICOM) using the theoretical foundation set forth by *Bleck and Boudra* [1981], *Bleck and Benjamin* [1993] and *Bleck* [2002]. This model has 1/12° horizontal resolution (~7 km at midlatitudes and 3.5 km at the North Pole) and 32 hybrid layers in the vertical, is isopycnal in the open stratified ocean and makes a smooth transition to a terrain-following (σ) coordinate in coastal waters using the layered continuity equation [*Bleck*, 2002]. The model's use of varying vertical coordinates allows it to effectively simulate the characteristics of ocean circulation as well as interior water mass distribution. These features are very important especially in the study of transport of ocean properties such as salinity as the dynamics are strongly influenced by localized processes hence the use of an entirely single vertical coordinate such as depth will be inefficient [*Chassignet et al.*, 1996]. The model is configured on a Mercator grid from 78°S to 47°N, while north of this latitude an Arctic dipole patch is used to avoid the singularity at the pole. HYCOM has the capability of selecting among several different vertical mixing submodels (e.g., K-Profile Parameterization [*Large et al.*, 1994] and Dynamical Instability Model [*Price et al*., 1986]) for either the surface mixed layer or the weak interior diapycnal mixing. This feature is essentially important for our study as salinity distribution, especially in the surface ocean is partly dependent on vertical mixing.

[11] Our version of HYCOM was initialized using monthly mean temperature and salinity from the 1/4° Generalized Digital Environmental Model (GDEM3) climatology [*NAVOCEANO*, 2003] in August. This experiment was then run for 13 years using climatological monthly mean wind and thermal forcing constructed from the 1.125° European Centre for Medium-Range Weather Forecasts (ECMWF) Re-Analysis (ERA15) over the 1979–1993 time frame. In addition, 6-hourly variability from the ECMWF operational model over the period September 1994–September 1995 was added to the climatological wind forcing (but not the thermal forcing) to add the higher-frequency variability needed for realistic simulation of the surface mixed layer. In order to keep the evaporation minus precipitation budget on track, the model weakly relaxes to monthly mean SSS from the Polar Science Center Hydrographic Climatology (PHC) SSS. This climatology is chosen for its accuracy in the Arctic region [*Steele et al.*, 2001]. The actual SSS relaxation e-folding time depends on the mixed layer depth (MLD) and is (30 days × 30 m/MLD m) days, i.e., it is more rapid when the MLD is shallow and less so when it is deep. The SSS relaxation is sufficient to avoid long-term drift in SSS, but not so strong as to inhibit SSS anomaly formation. The SSS relaxation is in addition to the evaporation-precipitation budget.

[12] Once the model was determined to be equilibrated after being spun-up with climatological forcing, the simulation was then continued using 3 hourly Navy Operational Global Atmospheric Prediction System (NOGAPS) winds, heat fluxes and precipitation fields for the period 2003–2006 as the forcing. This version of the model uses the NASA Goddard Institute for Space Studies level 2 (GISS) mixed layer scheme and includes monthly river runoff from 986 global rivers. There is no assimilation of any ocean data, including SST, and no relaxation to any other data except SSS to keep the evaporation minus precipitation balance on track.

[13] Because we are using the global version of HYCOM, there is no sponge layer across the lateral boundaries and the model allows the ITF to flow into the Indian Ocean and salt would be conserved. Also salt transport is estimated in various sigma t layers wherein it is expected that salt and mass are conserved and no attempt is placed to estimate the diapycnal mixing.

2.2. Data

[14] Climatological data sets on Evaporation and Precipitation for surface salinity variability analyses were obtained from the Hamburg Ocean Atmosphere Parameters and Fluxes from Satellite data set (HOAPS), Meteorological Institute of the University of Hamburg, Germany [*Anderson et al.*, 2007]. These parameters are generated from data obtained from the Special Sensor Microwave/Imager (SSM/I) radiometer aboard the Defense Meteorological Satellite Program (DMSP) satellites. The surface wind stress $\tau = \rho_a C_D \psi$ was computed from the Florida State University's (FSU) Center for Ocean-Atmosphere Prediction Studies (COAPS) 1° × 1° gridded pseudostress (ψ) data with ρ_a = 1.2041 kg/m^3 and C_D = 0.0015 [*Bourassa et al.*, 2005].

Table 1. HYCOM Layers With Approximate Depth

Layer	Mean Thickness (m)	Approximate Depth (m)
1	5	5
2	5	10
3	10	20
4	10	30
5	20	50
6	25	75
7	25	100
8	50	150
9	50	200
10	100	300
11	100	400
12	100	500
13	100	600
14	100	700
15	100	800
16	100	900
17	200	1100
18	200	1300
19	200	1500
20	200	1700
21	250	1950
22	250	2200
23	300	2500
24	300	2800
25	300	3100
26	500	3600
27	500	4100
28	500	4600
29	750	5350
30	750	6100
31	500	6600
32	500	7100

2.3. Methods

[15] *Hastenrath* [1984] summarizes the approach of estimating meridional transport as (a) evaluating the surface salinity budget and subsequently integrating with latitude to obtain transports across latitude circles, (b) directly evaluating transports from zonal hydrographic sections and (c) estimating the divergence of zonal transport by a major current (e.g., ACC) from meridional hydrographic sections. We chose the first approach as it will enable us to investigate the direct impact of seasonal reversal of winds and currents on surface ocean salinity variability and transport and then link it up to the subsurface transport. Additionally, the estimation of sea surface salinity transport from HYCOM will allow for future comparison with that estimated using satellite-derived surface salinity measurements from the European Space Agency (ESA) Soil Moisture and Ocean Salinity Mission (SMOS) and the future NASA Aquarius Salinity Mission.

[16] SSS transport in the Indian Ocean was computed from:

$$F_{sss} = \rho v S A \tag{1}$$

where F_{sss} is the surface salinity transport in 10^6 kg/s, ρ is the density of sea surface, 1023 kg/m^3, S is sea surface salinity (defined as $\times 10^{-3}$, hence the transport units of 10^6 kg/s), v is the meridional velocity in m/s, A is the cross-sectional area computed from $h \times l$, where h = 5 m (the depth of the first model layer) and l, the zonal extent of the cross-sectional area. For zonal surface salinity transport, v is replaced with u, the zonal velocity in m/s. The surface salinity transport is then connected to the subsurface ocean by computing depth-integrated salt transport across latitude circles using the HYCOM salinity along a section. In this regard, we compute salt transports along 5° latitudinal transects in the Indian Ocean using monthly mean HYCOM variables and equations from *Wijffels et al.* [1992], *Saunders and Thompson* [1993] and *Ganachaud et al.* [2000]:

$$F_s = \int_{-H}^{z_o} \int_{0}^{L} \rho . v(x,z) . S(x,z) dx dz \tag{2}$$

where F_s is the zonally integrated meridional salt transport in 10^6 kg/s, v is the meridional oceanic velocity in m/s and is perpendicular to the transect and positive for northward velocity, S is the spatially varying oceanic salinity, ρ is the density in kg/m^3 estimated from the potential density of the respective 32 isopycnal layers in the HYCOM, x and z are the zonal and vertical coordinates respectively, z_o is the ocean surface, H is the water depth in meters at a fixed position, x and L is the zonal expanse in meters of the ocean section at depth H. To compute the salt transport as per equation (2), information on the vertical distribution of salinity is required. To do this, we used the interface depth of the isopycnal layers in the HYCOM simulations, obtaining the approximate depths of the layers as shown in Table 1. Using isopycnal layers in the open ocean allows transport to follow surfaces of constant potential density in the Indian Ocean. It will also allow the interpretation of transport results with respect to water masses. Additionally, volume transport was computed to aid the interpretation and analyses of salt transport results; thus

$$F_v = \int_{-H}^{z_o} \int_{0}^{L} v(x,z) dx dz \tag{3}$$

where F_v is volume transport in Sv (1 Sv = 10^6 m^3 s^{-1}). For estimates of transports via the Indonesian Throughflow (ITF), the meridional velocity v in the above equations 2 and 3 is replaced with u, the zonal velocity and is positive for eastward velocity. Results of the computations are shown for 25°N to 35°S, where the Indian Ocean has an east and west landmass boundary.

[17] In an earlier study [*Nyadjro et al.*, 2010], Ekman component was reported to play a significant role in the distribution of salt in the sea surface. In this study, we analyze the effect of winds in salt transport in the Ekman layer by computing depth-integrated meridional Ekman transports using COAPS winds data. The annual mean meridional Ekman volume transport from HYCOM was computed following similar methods of *Levitus* [1988]:

$$Q_\phi = -\tau_\lambda / f \rho = \int_{-h}^{0} V_E dz \tag{4}$$

where Q_ϕ is the total horizontal Ekman transport, τ_λ is the zonal component of the wind stress, f is the Coriolis parameter and ρ is the density of seawater from HYCOM. V_E is the meridional Ekman velocity component and $-h$ is the depth of the Ekman boundary layer, which we chose to

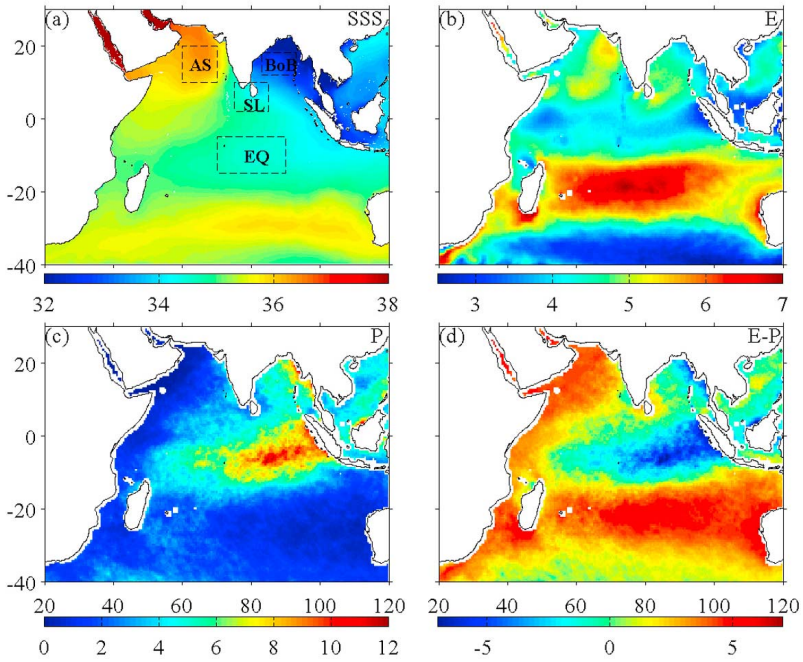

Figure 1. Mean annual (a) HYCOM SSS, (b) E (mm/day), (c) P (mm/day), and (d) E-P (mm/day) with boxes denoting the averaging subregions for surface salinity variability terms and surface salinity transport studies: Arabian Sea (AS), Bay of Bengal (BoB), Sri Lanka (SL), and Equatorial (EQ) regions.

be 100 m (~layer 7 of HYCOM). Meridional Ekman salt transport was computed from *Chereskin et al.* [2002]:

$$S_E = \int_{-H}^{z_o} \int_{0}^{L} \rho . V_E . S dx dz \tag{5}$$

where S_E is the meridional Ekman salt transport, S is HYCOM salinity.

[18] We compare our depth-integrated salt transport from HYCOM with that using the Simple Ocean Data Assimilation (SODA) model version 2.2.4 reanalysis output first described by *Giese and Ray* [2011]. This version of SODA combines an ocean model based on the Parallel Ocean Program (POP) version 2.0.1 numerics [*Smith et al.*, 1992] with hydrographic temperature and salinity data. SODA is a data-assimilated product and has a horizontal resolution that is on average 0.4° × 0.25° and with 40 levels in the vertical. The atmospheric reanalysis includes only surface observations of synoptic pressure and monthly SST and sea ice distribution from the Hadley Center Ice Sea Surface Temperature (HadISST v.1.1) data set [*Rayner et al.*, 2003]. The temperature and salinity profile data used in SODA was obtained from the recent release of the World Ocean Database 2009 (WOD09) [*Boyer et al.*, 2009].

3. Results and Discussion

3.1. Sea Surface Structures and Standard Deviation

[19] We present E, P, E-P results for spatially averaged data for the Arabian Sea (AS), Bay of Bengal (BoB), Sri Lanka (SL) and the Equatorial (EQ) regions which respectively are represented by the following boxes: AS (10°N to 20°N and 60°E to 70°E), BoB (12°N to 18°N and 83°E to 93°E), SL (2°N to 10°N and 75°E to 85°E) and equatorial (5°S to 15°S and 70°E to 90°E) (Figure 1a). These study regions are selected to reflect the different climatological and physical forcings in the Indian Ocean. Annual mean for SSS, E, P and E-P are respectively shown in Figures 1a–1d. SSS is highest in the AS and lowest in the BoB (Figure 1a) with the difference mainly as a result of E-P being greater in the former than the latter (Figure 1d). Although the annual mean evaporation seem to be similar for the two regions (Figure 1b), precipitation is greater in the BoB, especially during the SW monsoon. Additionally the high river runoff into the Bay also contributes to its lower salinity than the AS [*Sengupta et al.*, 2006]. The region south of the equator (10°S–30°S) shows the highest evaporation zone in the Indian Ocean (Figure 1b). Although the E-P in this region is similar to that of the AS (Figure 1d), SSS is lower here because of fresher water from the ITF [*Sengupta et al.*, 2006] while the AS additionally receives high saline waters from the Red and Persian Seas at subsurface depths.

[20] The temporal variability of the surface salinity variability terms, E, P and E-P are shown in Figure 2. On the average, precipitation is highest in the BoB and the EQ (Figures 2a and 2b) especially in the eastern ends of these regions (Figure 1c). Whereas in the EQ region it is consistently high throughout the years, that of the BoB shows significant seasonal variation. The annual mean and standard deviation respectively are 5.59 mm/day and 5.46 mm/day for the BoB and 6.50 mm/day and 1.87 mm/day for the EQ region. During the NE monsoon BoB precipitation is as low as < 1 mm/day but rises to about 15 mm/day at the peak of the SW monsoon with a month lag behind the precipitation peak in the AS. In the AS, precipitation shows seasonal

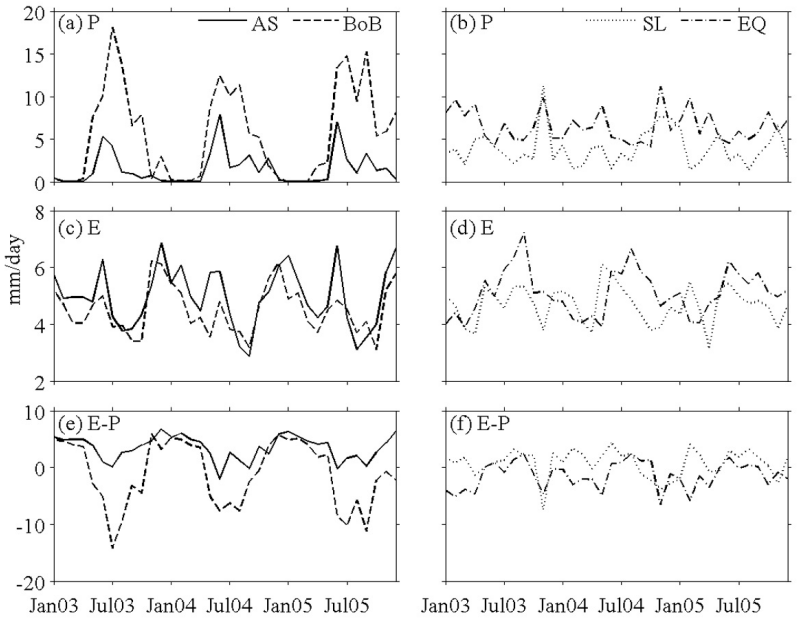

Figure 2. Temporal variability of surface salinity variability terms: (a, b) precipitation (P), (c, d) evaporation (E), and (e, f) E-P. Figures 2a, 2c, and 2e are for AS and BoB regions, while Figures 2b, 2d, and 2f are for SL and EQ regions.

variation with a near zero value throughout the NE monsoon season but peaks to about 5 mm/day during the SW monsoon season (Figure 2a). Annual mean and standard deviation for this region are 1.49 mm/day and 1.99 mm/day respectively. Precipitation in the SL region (Figure 2b) depicts a monthly sinusoidal pattern without a clear seasonal variation with annual mean and standard deviation being 3.94 mm/day and 2.12 mm/day.

[21] The evaporation term shows seasonal variation in all the study regions (Figures 2c and 2d). During the NE monsoon and at the start of the SW monsoon, evaporation in the four regions are all in phase. At the peak of the SW monsoon, however, that of SL and EQ increases while it decreases in the AS and BoB regions. The annual mean and standard deviation respectively are 4.68 mm/day and 0.67 mm/day for the SL and 5.11 mm/day and 0.82 mm/day for the EQ region. The AS has an annual mean of 4.96 mm/day and a standard deviation of 1.06 mm/day while for the BoB it is 4.51 mm/day and 0.82 mm/day respectively. The AS region (Figure 2c) shows annual bimodal peaks occurring in June and December with the former coinciding with the minima E-P and the latter with the maxima E-P in the AS region (Figure 2e).

[22] The largest variation in the E-P term is seen in the BoB (Figure 2e) where the temporal distribution generally is a mirror image of the P variations in the BoB, an indication of the controlling role of precipitation in this region and the effect it has on salinity flux. The annual mean E-P is −1.07 mm/day with a high standard deviation of 5.79 mm/day. The net flux can reach −15 mm/day in July, implying an input of freshwater into the basin. Along the EQ region (Figure 2f) too, the E-P distribution mimics the mirror image of P with a mean of −1.40 mm/day and a standard deviation of 2.43 mm/day. The flux of freshwater into this region is from the Indonesian Throughflow (ITF), Inter Tropical Convergence Zone (ITCZ) rainfall and freshwater transported from the BoB [*Joseph and Freeland*, 2005; *Sengupta et al.*, 2006]. E-P is highest in the AS (Figure 2e) with a mean of 3.47 mm/day and a standard deviation of 2.17 mm/day. This reflects the minimal influence of freshwater in the distribution of SSS in this basin.

3.2. Surface Flow Velocity Structure

[23] In this section, we describe the structure of the HYCOM simulated surface flow velocities. The zonal component shows significant seasonal variability in the study regions except in the EQ region, where it is minimal (Figures 3a–3d). Surface flow is eastward during the SW monsoon at which time the maximum velocities are also observed. Surface flow is westward during the NE monsoon in all the study regions except the EQ region, where it is westward during the SW monsoon months and becomes eastward (decrease of negative westward velocity) by April/May under the influence of equatorial jets (Figure 3d). The meridional component of the flow shows significant seasonal variation only in the SL region (Figure 3c). Overall, the strongest velocities are seen in the SL region (Figure 3c) emphasizing its role in the exchange of salt and mass between the AS and BoB. The seasonal reversing of these velocities affects the currents and hence the transport of water and salt. It also contributes to the seasonal variation in the SSS transport that is observed especially in the northern Indian Ocean.

3.3. Seasonal Variation of SSS Transport

[24] Results for meridional and zonal surface salinity transport magnitudes are shown in Figure 4. The patterns of magnitude and direction of the surface salt transport track

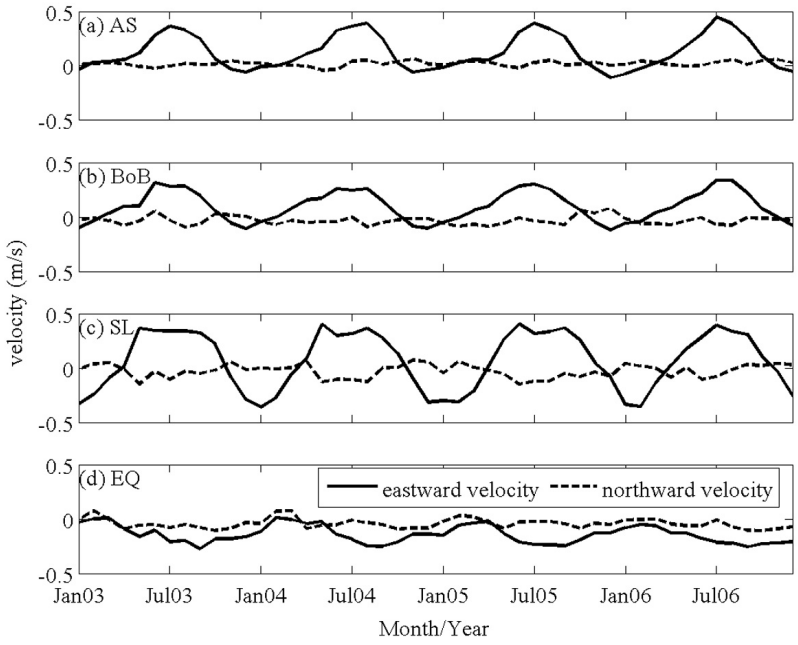

Figure 3. Seasonal variation of surface velocity flow in the Arabian Sea (AS), Bay of Bengal (BoB), Sri Lanka (SL), and Equatorial (EQ) regions.

that of the surface flow velocity (Figure 3). Zonal transports are higher and show larger seasonal variation than meridional transport in all the study regions (Figure 4). In the AS and BoB regions (Figures 4a and 4b), zonal SSS transport is maximum (0.75×10^6 kg s^{-1}) and eastward during the peak of the SW monsoon. Transport becomes westward during the NE monsoon season but of lesser magnitude (maximum of -0.2×10^6 kg s^{-1}) than during the SW monsoon season. The westward flow in the BoB during winter is responsible for the transport of low-saline water via the North Equatorial Current into the AS. In the SL region (Figure 4c), maximum zonal salt transport (0.5×10^6 kg s^{-1}) occurs at the peak of the monsoons and of similar magnitudes but reversed directions. It is westward and eastward respectively during the NE and SW monsoons. In the EQ region (Figure 4d), zonal surface salinity transports are almost entirely westward

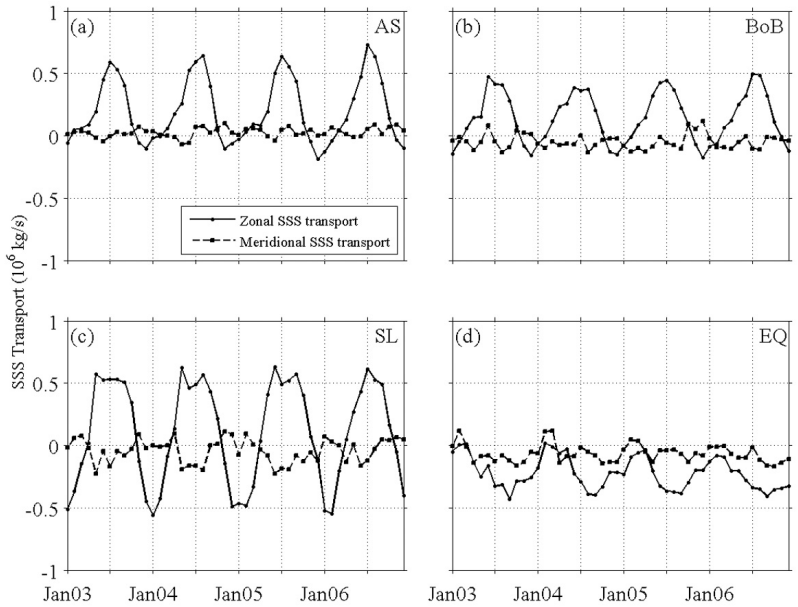

Figure 4. Seasonal variation of area-averaged zonal and meridional surface salinity transport for the (a) Arabian Sea (AS), (b) Bay of Bengal (BoB), (c) Sri Lanka (SL), and (d) Equatorial (EQ) regions.

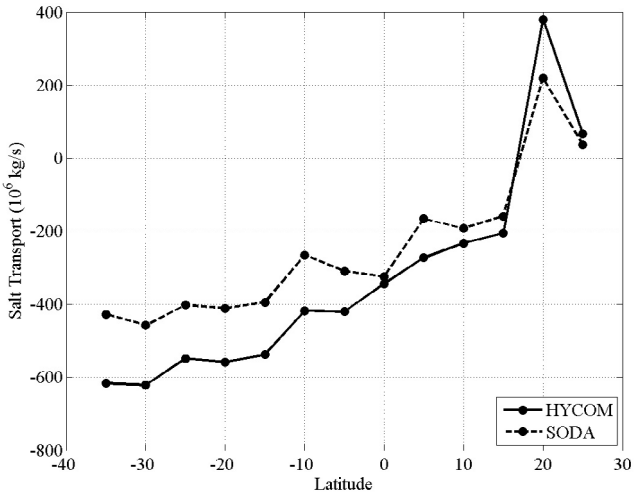

Figure 5. Comparison of latitudinal variation of net meridional depth-integrated salt transport computed using HYCOM and SODA.

with maximum (-0.45×10^6 kg s^{-1}) occurring in September, at the end of the SW monsoon season while the minimum (0.05×10^6 kg s^{-1}) occurs in February, at the end of the NE monsoon season. Meridional SSS transport is northward in the AS during the NE and SW monsoon seasons with maximum (~0.1×10^6 kg s^{-1}) observed at the peak of the monsoons. It is, however, southward during the pre-SW monsoon, where it reaches -0.1×10^6 kg s^{-1} in May. In the BoB, meridional transport is mostly southward during the SW monsoon season and at the start of the NE monsoon season but reverses to southward at the peak of the later season. The largest meridional SSS transport occurs in the SL region, where it is northward during the NE monsoon season with a peak of about 0.1×10^6 kg s^{-1}. During the SW monsoon season, the transport reverses, becoming southward and peaking at about -0.2×10^6 kg s^{-1} toward the end of that season. In the EQ region, meridional SSS transport fairly tracks that of the zonal transport and is mainly southward with northward transport observed only at the end of the NE monsoon season.

3.4. Depth-Integrated Meridional Salt Transport

[25] Depth-integrated meridional salt transport computed using HYCOM are compared to that using SODA (a data assimilated product) with the results (Figure 5) showing they track each other quite reasonably in sign and magnitude. The annual mean estimates of HYCOM net meridional salt transport in the Indian Ocean (Figure 6) indicate a

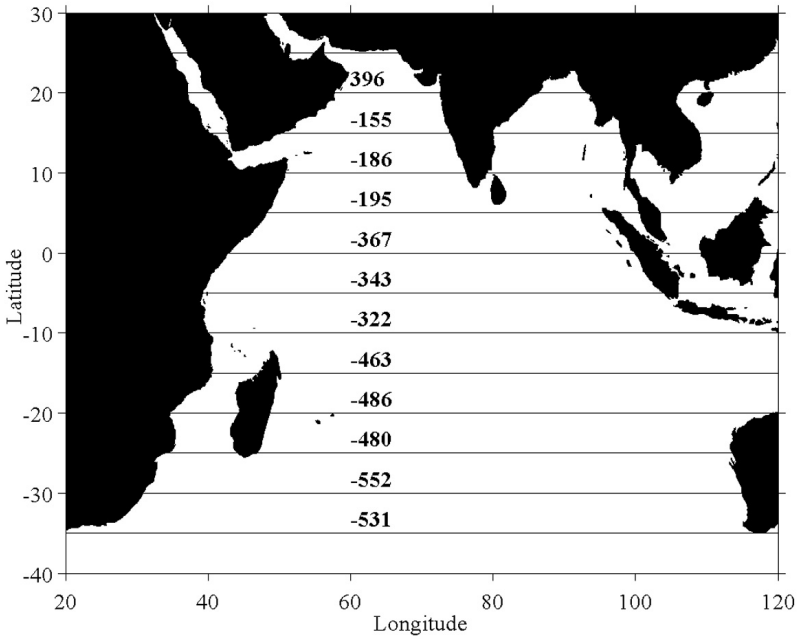

Figure 6. Annual mean depth-integrated net meridional salt transport ($\times 10^6$ kg/s) for each 5° latitudinal belt in the Indian Ocean.

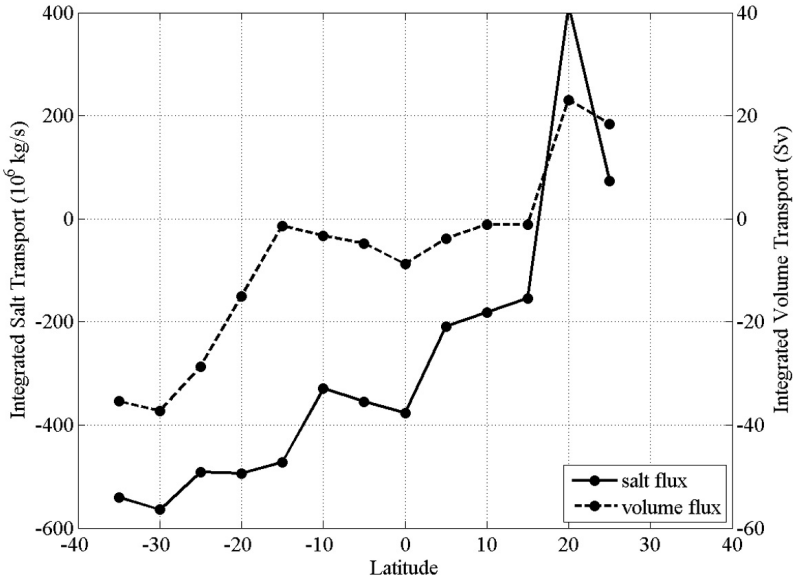

Figure 7. Latitudinal variation of depth-integrated meridional salt and volume transport in the Indian Ocean computed from 4 year mean HYCOM simulations.

southward transport at all latitudes except 20°N, where it is 396 × 10^6 kg/s. It generally increases southward with the highest transports (−463 × 10^6 kg/s to −531 × 10^6 kg/s) occurring in the south (10°S–35°S) and a maximum of −552 × 10^6 kg/s at 30°S. The northern salt transport at 20°N may be due to the shallowness of the bottom topography and all the layers would not be considered as that at for example 20°S or 30°S, where the ocean is deep. This northward salt transport at 20°N and southward salt transport at 15°N in the Arabian Sea would lead to salt divergence between 15°N and 20°N and we do not have any immediate explanation for this. Probably, this is an important feature that leads to the flow of high-salinity water masses of Persian Gulf origin and Red Sea origin at subsurface depths and also compensates the net salt loss due to predominant evaporation than precipitation and no river runoff. The southward direction of salt transport in the Indian Ocean is consistent with the study of *Toole and Warren* [1993] where they obtained a net salt flux of −236.8 × 10^6 kg/s at 32°S.

[26] The net salt and volume flux track each other quite closely at all latitude except between 5°S and 20°S, where there is a significant difference in the patterns (Figure 7). This is as a result of large volume of water from the ITF. This water is, however, less saline and therefore does not significantly increase the magnitude of salinity in that region.

[27] Sectionally integrated salt fluxes showing contributions from each layer are shown in Figure 8. In the northern Indian Ocean, at 20°N (Figure 8a), southward transports are seen only in deep waters with the rest of the water column showing northward flux. The net flux of salt at this latitude is northward. The flow is southward in almost all layers at 10°N (Figure 8b) with a northward transport between layers 12–15. Generally for the Southern Indian Ocean (Figures 8d–8f), surface and deep water layers show southward transport while intermediate and bottom water layers show northward transport. Net fluxes for the entire sections, however, show a northward salt transport of bottom waters and a southward salt transport of surface waters. When considered as a whole, the Indian Ocean shows a net southward transport of salt. Plots of depth-integrated volume transport (Figures 9a–9f) show that they track that of the salt-integrated transport closely in both magnitude and direction.

[28] Freshwater flux mainly directly affects distribution and variability of surface salinity [*Wijffels et al.*, 1992; *Rao and Sivakumar*, 2003]. In the deeper regions of the Indian Ocean, salt distribution is influenced by water transported into it from other oceans. Deep water is not formed in the Indian Ocean but rather they originate from the Atlantic and Southern Oceans. Localized deep water is only formed by mixing [*Mantyla and Reid*, 1995]. As a result, the Indian Ocean converts cold dense water to warm surface waters, a direct opposite to what happens in the Atlantic Ocean. Portions of the southward flowing North Atlantic Deep Water that fails to be incorporated into the thermocline of the Atlantic flows eastward with the Antarctic Circumpolar Current (ACC) into the Indian and Pacific Oceans [*Gordon*, 1986; *Rintoul*, 1991]. Part of the NADW that enters the Pacific Ocean is later transported into the Indian Ocean via the ITF, the water of which flows westward courtesy the South Equatorial Current (SEC), all the way to the Mozambique Channel. Along this transport route, large-scale upwelling returns the high-saline deep waters to the surface, significantly changing the salt content of the Indian Ocean [*Stommel*, 1958; *Gordon*, 1986; *van Aken et al.*, 2004].

[29] The ITF plays important role in the distribution of salt in the Indian Ocean. Its strength influences the salinity budget as far west as the Somali Current region [*Godfrey*, 1996; *Gordon et al.*, 1999; *Potemra*, 2005]. In this study, we obtained an ITF volume flux of 14.4 Sv into the Indian Ocean; a value close to *Piola and Gordon*'s [1984] 14 Sv. Other estimates include 12 Sv [*Godfrey*, 1989], 7 Sv [*Fu*,

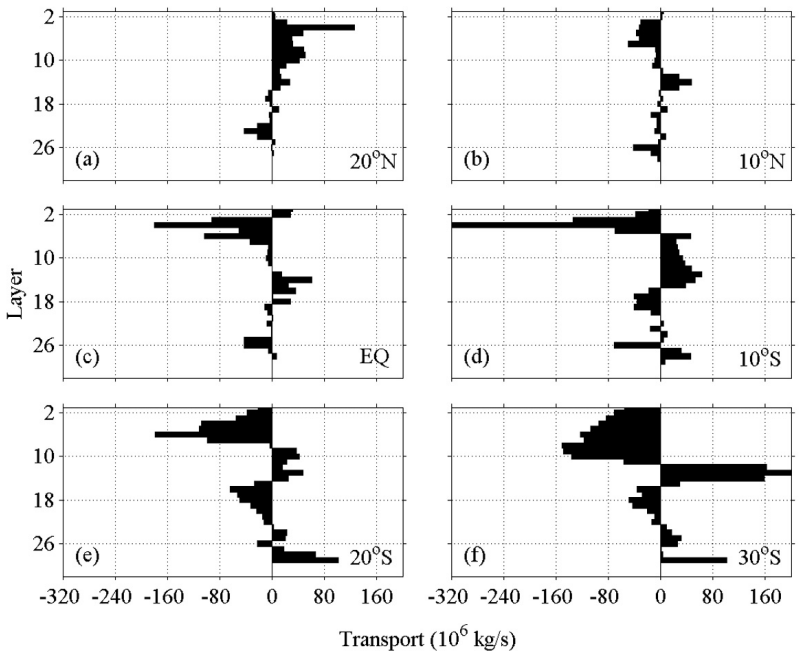

Figure 8. Depth-integrated meridional salt transport in each layer integrated along latitudinal sections in the Indian Ocean computed from 4 year mean HYCOM simulations. Positive transport is to the north.

1986], and 18.6 Sv [*Fieux et al.*, 1994]. The different values underscore the difficulty in estimating the ITF as a result of its complex topography and large variation in tides [*Potemra*, 2005; *Valsala and Ikeda*, 2007]. It also could imply a large seasonal and interannual variation of the ITF [*Godfrey*, 1996]. From the HYCOM estimates, the bulk of the ITF flux occurs in the top 18 model layers representing about 800 m (Figure 10). This pattern tracks that of the salt flux which shows a net flux of 512.2 × 10^6 kg s^{-1} into the Indian Ocean.

[30] There is higher transport at higher latitudes in the Indian Ocean. The largest seasonal variation (January and July compared) in net meridional salt transport is seen closer to the equatorial region; between 10°S and 20°N, with the

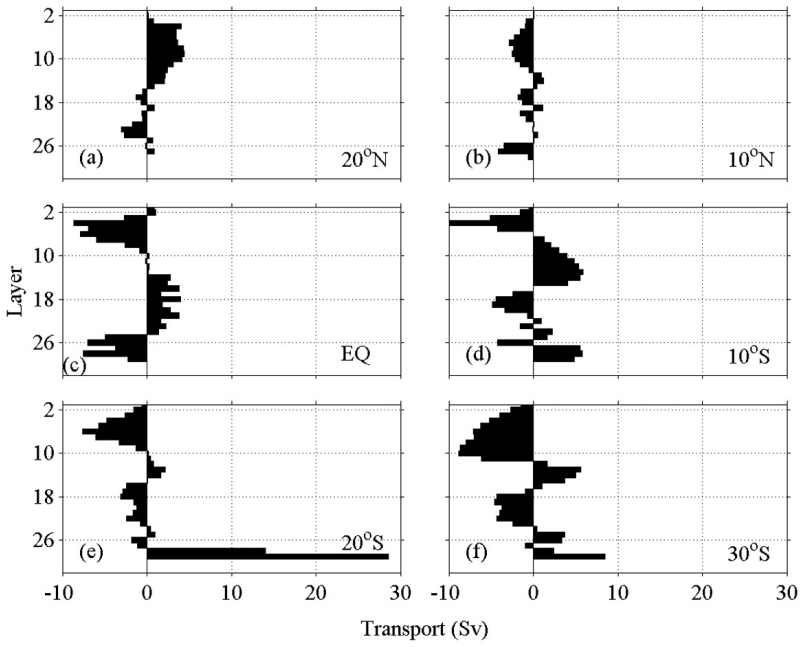

Figure 9. Depth-integrated meridional volume transport (1 Sv = 10^6 m^3 s^{-1}) in each layer integrated along latitudinal sections in the Indian Ocean. Positive transport is to the north.

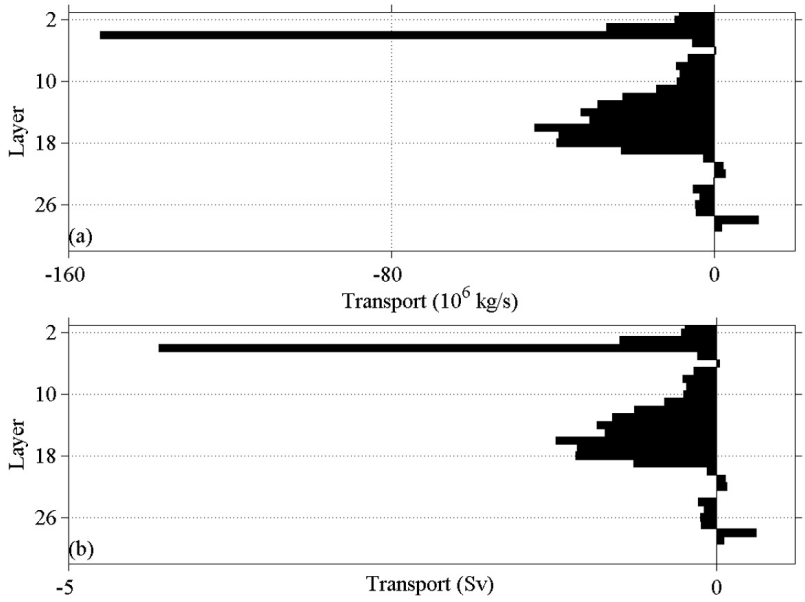

Figure 10. Depth-integrated zonal (a) salt and (b) volume transport in each layer integrated along the ITF region. Positive fluxes are to the east.

largest occurring at 10°S and 10°N (Figure 11). Currents southward of 10°S do not show much seasonal variability as compared to those northward of 10°S [*Schott and McCreary*, 2001]. At the southernmost extent of the Indian Ocean, there is not much variability in the salt flux. Between 15°S and 35°S, the seasonal values are almost the same. Between 15°S and 15°N, the net flux is southward and July salt flux is generally lower than the annual mean salt flux while January salt flux is generally higher than the annual mean. From 20°N to 25°N, however, the net flux is northward and July flux is higher than the annual mean while the January flux is lower than the annual mean. Flux decreases as latitude decreases from the south to the north. The northern flux is weaker as the effect of freshwater flux "dilutes" the water. For the entire study period (2003–2006), the monthly mean salt transport (Figure 12) at the selected latitudes south of the equator show year-round southward flux. Northward of the equator and especially at 20°N,

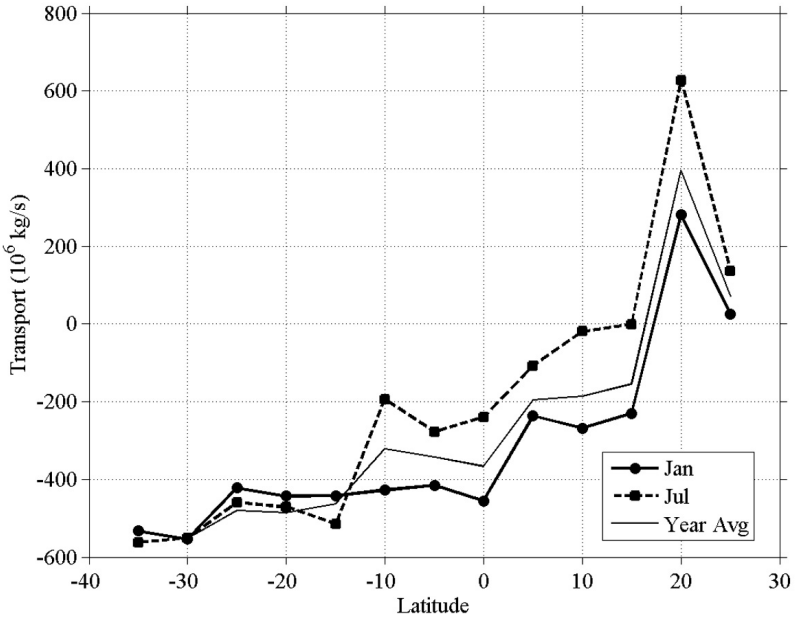

Figure 11. Seasonal variation of net depth-integrated meridional salt transport in the Indian Ocean computed from 4 year mean January and July simulations. Positive transport is to the north.

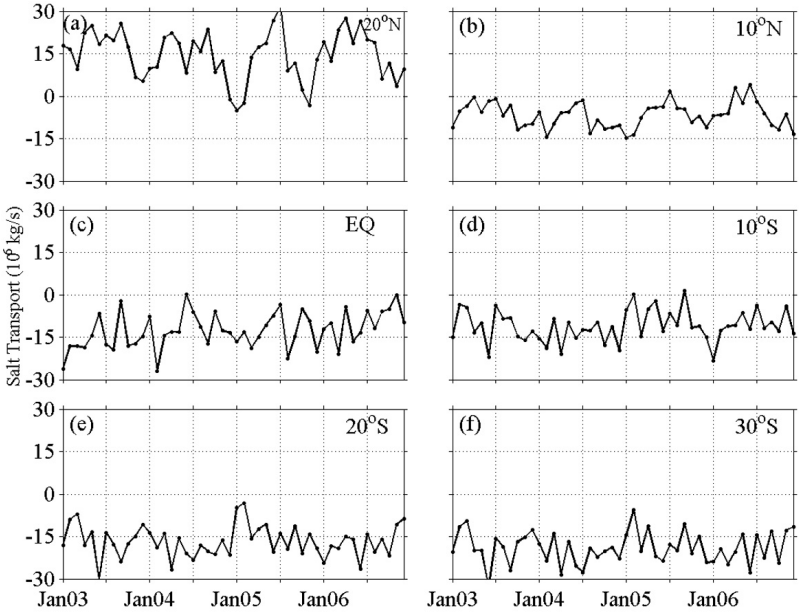

Figure 12. Seasonal variation of depth-integrated meridional salt transport in each layer integrated along latitudinal sections in the Indian Ocean. Positive transport is to the north.

northward transports are observed in some months. At 10°S, 20°S and 30°S, maximum meridional transport (-30×10^6 kg s^{-1}) occurs in June, at the start of SW monsoon. During the NE monsoon season, the transports are more toward the equator while being more toward the poles during the SW monsoon season.

[31] Our estimates of meridional Ekman volume and salt transport (Figure 13) show a net southward transport in the Indian Ocean. This trend in the Indian Ocean has been attributed to the strong summer monsoon southwesterly winds [*Levitus*, 1988; *Chereskin et al.*, 2002]. The volume transport magnitude and direction is close to that of *Levitus* [1988], who showed similar magnitudes and directions. The annual mean meridional Ekman volume transport is northward (~0.4 Sv) only at 20°N. Equatorward of 20°N, it becomes increasingly southward between reaching a maximum of about 10 Sv at 2°30′N. No data is presented between 2°30′N and 2°30′S as a result of the absence of Coriolis near the equator. In the southern Indian Ocean, meridional Ekman volume transport increases poleward

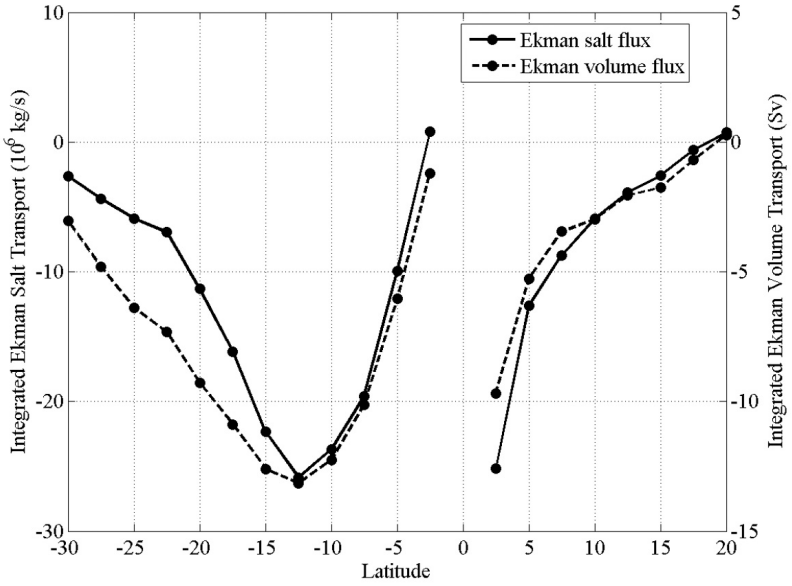

Figure 13. Annual mean latitudinal variation of depth-integrated Ekman meridional salt and volume transport in the Indian Ocean.

from about −0.5 Sv until it reaches a maximum of about 13 Sv at 12°30′S. *Levitus* [1988] reported a maximum of ~18 Sv at 11°N. Southward of 12°30′S, the Ekman meridional volume transport is still southward but of lesser magnitude. The meridional Ekman salt transport tracks that of the volume closely, with a maximum (25×10^6 kg s^{-1}) occurring at 12°S. A secondary maximum of ~24×10^6 kg s^{-1} occurs at 2°30′N. A positive Ekman salt transport (~1×10^6 kg s^{-1}) is observed at 2°30′N. The reduced meridional Ekman transports observed southward of 12°30′S can be attributed to the lesser impact of monsoon winds in that region.

4. Conclusions

[32] In this paper, 4 year HYCOM simulations are used to study the transport of salinity in the surface layers of the Indian Ocean and to estimate the flux of salt in the 32 HYCOM layers using depth-integrated transport methods. Results show the temporal and spatial variability of surface salinity variability terms among the four subregions studied. Precipitation is highest in the Bay of Bengal while showing a sinusoidal pattern in the Sri Lankan region. Although evaporation is high in the Arabian Sea, seasonal variation is quite minimal in the study regions with annual bimodal peaks in the AS coinciding with the minima and maxima respectively of E-P. Zonal SSS transport was larger than meridional SSS transport. The strongest variability is seen in the SL region while in the EQ, SSS transport was almost entirely southward and westward respectively. Depth-integrated transport studies showed a northward transport of volume and salt in bottom water layers and a southward transport of salt in surface layers. The highest net salt flux of -552×10^6 kg/s is observed at 30°S, a region influenced by the Circumpolar Deep Water and the Antarctic Bottom Water. Seasonal variation in salt flux is significantly noticeable along the equatorial region where ITCZ influences rain patterns and as well as influence by the ITF. The ITF transports about 14.4 Sv of water and 512.2×10^6 kg s^{-1} of salt into the Indian Ocean. Overall, there is a net southward flux of salt in almost all latitudes of the Indian Ocean with patterns reflecting the transport of water masses and currents in the Ocean. Analyses of meridional Ekman volume and salt transport show a predominantly southward transport, an indication of the strong influence of SW monsoonal winds. This study illustrates that the HYCOM output is useful for calculating Indian Ocean salinity transport and should be useful in computing near-surface salt transport from the Soil Moisture and Ocean Salinity (SMOS) and Aquarius satellite missions as well.

[33] **Acknowledgments.** This work was supported by the Office of Naval Research (ONR) Award N000141110700 awarded to B.S. J.S. was supported by the 6.1 project "Global and Remote Littoral Forcing in the Global Ocean Models" sponsored by the Office of Naval Research (ONR) under the program element 601153N. The authors would like to thank two anonymous reviewers for all their helpful comments and suggestions.

References

Anderson, A., S. Bakan, K. Fenning, H. Grassel, C.-P. Klepp, and J. Schluz (2007), Hamburg Ocean Atmosphere Parameters and Fluxes from Satellite Data—HOAPS—3-monthly mean, doi:10.1594/WDCC/HOAPS3_MONTHLY, World Data Cent. for Clim, Hamburg, Germany.

Bleck, R. (2002), An oceanic general circulation model framed in hybrid isopycnic-Cartesian coordinates, *Ocean Modell.*, *4*, 55–88, doi:10.1016/S1463-5003(01)00012-9.

Bleck, R., and S. G. Benjamin (1993), Regional weather prediction with a model combining terrain-following and isentropic coordinates. I: Model description, *Mon. Weather Rev.*, *121*(6), 1770–1785, doi:10.1175/1520-0493(1993)121<1770:RWPWAM>2.0.CO;2.

Bleck, R., and D. B. Boudra (1981), Initial testing of a numerical ocean circulation model using a hybrid (quasi-isopycnic) vertical coordinate, *J. Phys. Oceanogr.*, *11*(6), 755–770, doi:10.1175/1520-0485(1981)011<0755:ITOANO>2.0.CO;2.

Bourassa, M. A., R. Romero, S. Smith, and J. O'Brien (2005), A new FSU winds climatology, *J. Clim.*, *18*, 3686–3698, doi:10.1175/JCLI3487.1.

Boyer, T. P., et al. (2009), *World Ocean Database 2009* [DVDs], *NOAA Atlas NESDIS*, vol. 66, edited by S. Levitus, 216 pp., U.S. Govt. Print. Off., Washington, D. C.

Chassignet, E. P., L. T. Smith, R. Bleck, and F. O. Bryan (1996), A model comparison: Numerical simulations of the north and equatorial Atlantic Oceanic circulation in depth and isopycnic coordinates, *J. Phys. Oceanogr.*, *26*(9), 1849–1867, doi:10.1175/1520-0485(1996)026<1849:AMCNSO>2.0.CO;2.

Chereskin, T. K., W. D. Wilson, and L. M. Beal (2002), The Ekman temperature and salt fluxes at 8°30′N in the Arabian Sea during the 1995 southwest monsoon, *Deep Sea Res., Part II*, *49*, 1211–1230, doi:10.1016/S0967-0645(01)00168-0.

Czaja, A. (2009), Atmospheric control on the thermohaline circulation, *J. Phys. Oceanogr.*, *39*, 234–247, doi:10.1175/2008JPO3897.1.

Delcroix, T., and C. Henin (1991), Seasonal and interannual variations of the sea surface salinity in the tropical Pacific Ocean, *J. Geophys. Res.*, *96*, 22,135–22,150, doi:10.1029/91JC02124.

Delcroix, T., C. Henin, V. Porte, and P. Arkin (1996), Precipitation and sea surface salinity in the tropical Pacific Ocean, *Deep Sea Res., Part I*, *43*(7), 1123–1141, doi:10.1016/0967-0637(96)00048-9.

Donguy, J. E., and G. Meyers (1996), Seasonal variations of sea surface salinity and temperature in the tropical Indian Ocean, *Deep Sea Res., Part I*, *43*(2), 117–138, doi:10.1016/0967-0637(96)00009-X.

Dourado, M., and G. Caniaux (2003), Surface salinity budget in oceanic simulation using data from TOGA COARE, *J. Geophys. Res.*, *108*(C5), 3135, doi:10.1029/2001JC001013.

Durand, F., D. Shankar, C. de Boyer Montégut, S. S. C. Shenoi, B. Blanke, and G. Madec (2007), Modelling the barrier-layer formation in the south-eastern Arabian Sea, *J. Clim.*, *20*, 2109–2120, doi:10.1175/JCLI4112.1.

Esenkov, O. E., D. Olson, and R. Bleck (2003), A study of the circulation and salinity budget of the Arabian Sea with an isopycnic coordinate ocean model, *Deep Sea Res., Part II*, *50*, 2091–2110, doi:10.1016/S0967-0645(03)00047-X.

Fieux, M., C. Andrie, P. Delecluse, A. G. Ilahude, A. Kartavseff, F. Mantisi, R. Molcard, and J. C. Swallow (1994), Measurements within the Pacific-Indian oceans throughflow region, *Deep Sea Res., Part I*, *41*, 1091–1130, doi:10.1016/0967-0637(94)90020-5.

Foltz, G. R., and M. J. McPhaden (2008), Seasonal mixed layer salinity balance of the tropical North Atlantic Ocean, *J. Geophys. Res.*, *113*, C02013, doi:10.1029/2007JC004178.

Fu, L.-L. (1986), Mass, heat and freshwater fluxes in the south Indian Ocean, *J. Phys. Oceanogr.*, *16*, 1683–1693, doi:10.1175/1520-0485(1986)016<1683:MHAFFI>2.0.CO;2.

Ganachaud, A., C. Wunsch, J. Marotzke, and J. Toole (2000), Meridional overturning and large-scale circulation of the Indian Ocean, *J. Geophys. Res.*, *105*(C11), 26,117–26,134, doi:10.1029/2000JC900122.

Giese, B. S., and S. Ray (2011), El Niño variability in simple ocean data assimilation (SODA), 1871–2008, *J. Geophys. Res.*, *116*, C02024, doi:10.1029/2010JC006695.

Godfrey, J. (1996), The effect of the Indonesian throughflow on ocean circulation and heat exchange with the atmosphere: A review, *J. Geophys. Res.*, *101*(C5), 12,217–12,237, doi:10.1029/95JC03860.

Godfrey, J. S. (1989), A Sverdrup model of the depth-integrated flow for the world ocean allowing for island circulations, *Geophys. Astrophys. Fluid Dyn.*, *45*, 89–112, doi:10.1080/03091928908208894.

Gordon, A. (1986), Interocean exchange of thermocline water, *J. Geophys. Res.*, *91*(C4), 5037–5046, doi:10.1029/JC091iC04p05037.

Gordon, A. L., R. F. Weiss, W. M. Smethie Jr., and M. J. Warner (1992), Thermocline and intermediate water communication between the South Atlantic and Indian oceans, *J. Geophys. Res.*, *97*(C5), 7223–7240, doi:10.1029/92JC00485.

Gordon, A. L., R. D. Susanto, and A. Ffield (1999), Throughflow within Makassar Strait, *Geophys. Res. Lett.*, *26*(21), 3325–3328, doi:10.1029/1999GL002340.

Gründlingh, M. L. (1985), Occurrence of Red Sea Water in the south-western Indian Ocean, 1981, *J. Phys. Oceanogr.*, *15*, 207–212, doi:10.1175/1520-0485(1985)015<0207:OORSWI>2.0.CO;2.

Han, W., and J. P. McCreary (2001), Modeling salinity distributions in the Indian Ocean, *J. Geophys. Res.*, *106*, 859–877, doi:10.1029/2000JC000316.

Han, W., J. McCreary Jr., and K. Kohler (2001), Influence of precipitation minus evaporation and Bay of Bengal rivers on dynamics, thermodynamics, and mixed layer physics in the upper Indian Ocean, *J. Geophys. Res.*, *106*(C4), 6895–6916, doi:10.1029/2000JC000403.

Hareesh Kumar, V. H., M. Joshi, K. V. Sanilkumar, A. D. Rao, P. Anand, K. A. Kumar, and C. V. K. P. Rao (2009), Growth and decay of the Arabian Sea mini warm pool during May 2000: Observations and simulations, *Deep Sea Res., Part I*, *56*, 528–540, doi:10.1016/j.dsr.2008.12.004.

Hastenrath, S. (1984), On the meridional transports of heat and freshwater in the Pacific Ocean, *Meteorol. Atmos. Phys.*, *33*, 91–99.

Illig, S., and C. Perigaud (2007), Yearly impact of submonthly rain fluctuations on the Indian Ocean salinity, *Geophys. Res. Lett.*, *34*, L12609, doi:10.1029/2007GL029655.

Jensen, T. G. (2001), Arabian Sea and Bay of Bengal exchange of salt and tracers in an ocean model, *Geophys. Res. Lett.*, *28*, 3967–3970, doi:10.1029/2001GL013422.

Joseph, S., and H. J. Freeland (2005), Salinity variability in the Arabian Sea, *Geophys. Res. Lett.*, *32*, L09607, doi:10.1029/2005GL022972.

Large, W. G., J. C. McWilliams, and S. C. Doney (1994), Oceanic vertical mixing: A review and a model with a nonlocal boundary layer parameterization, *Rev. Geophys.*, *32*(4), 363–403, doi:10.1029/94RG01872.

Levitus, S. (1988), Ekman volume fluxes for the world ocean and individual ocean basins, *J. Phys. Oceanogr.*, *18*, 271–279, doi:10.1175/1520-0485(1988)018<0271:EVFFTW>2.0.CO;2.

Mantyla, A. W., and J. L. Reid (1995), On the origins of deep and bottom waters of the Indian Ocean, *J. Geophys. Res.*, *100*(C2), 2417–2439, doi:10.1029/94JC02564.

Morrison, J. (1997), Inter-monsoonal changes in the T-S properties of the near-surface waters of the northern Arabian Sea, *Geophys. Res. Lett.*, *24*, 2553–2556, doi:10.1029/97GL01876.

Murtugudde, R., and A. J. Busalacchi (1998), Salinity effects in a tropical ocean model, *J. Geophys. Res.*, *103*(C2), 3283–3300, doi:10.1029/97JC02438.

Murtugudde, R., R. Seager, and P. Thoppil (2007), Arabian Sea response to monsoon variations, *Paleoceanography*, *22*, PA4217, doi:10.1029/2007PA001467.

NAVOCEANO (2003), Database description for the generalized digital environmental model (GDEM-V) Version 3.0.OAML-DBD-72, report, 34 pp., NAVOCEANO Oceanogr. Data Bases Div., Stennis Space Center, Miss.

Nyadjro, E. S., B. Subrahmanyam, V. S. N. Murty, and J. F. Shriver (2010), Salt transport in the near-surface layer in the monsoon-influenced Indian Ocean using HYCOM, *Geophys. Res. Lett.*, *37*, L15603, doi:10.1029/2010GL044127.

Oka, A., and H. Hasumi (2006), Effects of model resolution on salt transport through northern high-latitude passages and Atlantic meridional overturning circulation, *Ocean Modell.*, *13*, 126–147, doi:10.1016/j.ocemod.2005.12.004.

Piola, A. R., and A. L. Gordon (1984), Pacific and Indian Ocean upper-layer salinity budget, *J. Phys. Oceanogr.*, *14*, 747–753, doi:10.1175/1520-0485(1984)014<0747:PAIOUL>2.0.CO;2.

Potemra, J. T. (2005), Indonesian Throughflow transport variability estimated from satellite altimetry, *Oceanography*, *18*(4), 98–107.

Prasad, T. G., and M. Ikeda (2002a), The wintertime water mass formation in the northern Arabian Sea: A model study, *J. Phys. Oceanogr.*, *32*, 1028–1040, doi:10.1175/1520-0485(2002)032<1028:TWWMFI>2.0.CO;2.

Prasad, T. G., and M. Ikeda (2002b), A numerical study of the seasonal variability of Arabian Sea high-salinity water, *J. Geophys. Res.*, *107*(C11), 3197, doi:10.1029/2001JC001139.

Prasanna Kumar, S., et al. (2004), Intrusion of the Bay of Bengal water into the Arabian Sea during winter monsoon and associated chemical and biological response, *Geophys. Res. Lett.*, *31*, L15304, doi:10.1029/2004GL020247.

Price, J. F., R. A. Weller, and R. Pinkel (1986), Diurnal cycling: Observations and models of the upper ocean response to diurnal heating, cooling, and wind mixing, *J. Geophys. Res.*, *91*(C7), 8411–8427, doi:10.1029/JC091iC07p08411.

Rajamani, V., U. C. Mohanty, R. Ramesh, G. S. Bhat, P. N. Vinayachandran, D. Sengupta, S. Prasanna Kumar, and R. K. Kolli (2006), Linking Indian rivers vs. Bay of Bengal monsoon activity, *Curr. Sci.*, *90*(1), 12–13.

Rao, R. R., and R. Sivakumar (2003), Seasonal variability of sea surface salinity and salt budget of the mixed layer of the north Indian Ocean, *J. Geophys. Res.*, *108*(C1), 3009, doi:10.1029/2001JC000907.

Rayner, N. A., D. E. Parker, E. B. Horton, C. K. Folland, L. V. Alexander, D. P. Rowell, E. C. Kent, and A. Kaplan (2003), Global analyses of sea surface temperature, sea ice, and night marine air temperature since the late nineteenth century, *J. Geophys. Res.*, *108*(D14), 4407, doi:10.1029/2002JD002670.

Rintoul, S. (1991), South Atlantic interbasin exchange, *J. Geophys. Res.*, *96*(C2), 2675–2692, doi:10.1029/90JC02422.

Saunders, P. M., and S. R. Thompson (1993), Transport, heat and freshwater fluxes within a diagnostic numerical model (FRAM), *J. Phys. Oceanogr.*, *23*, 452–464, doi:10.1175/1520-0485(1993)023<0452:THAFFW>2.0.CO;2.

Schott, F., and J. P. McCreary (2001), The monsoon circulation of the Indian Ocean, *Prog. Oceanogr.*, *51*, 1–123, doi:10.1016/S0079-6611(01)00083-0.

Sengupta, D., G. N. Bharath Raj, and S. S. C. Shenoi (2006), Surface freshwater from Bay of Bengal runoff and Indonesian Throughflow in the tropical Indian Ocean, *Geophys. Res. Lett.*, *33*, L22609, doi:10.1029/2006GL027573.

Sévellec, F., T. Huck, M. B. Jelloul, N. Grima, J. Vialard, and A. Weaver (2008), Optimal surface salinity perturbations of the meridional overturning and heat transport in a global ocean general circulation model, *J. Phys. Oceanogr.*, *38*, 2739–2754, doi:10.1175/2008JPO3875.1.

Smith, R. D., J. K. Dukowicz, and R. C. Malone (1992), Parallel ocean general circulation modeling, *Physica D*, *60*, 38–61, doi:10.1016/0167-2789(92)90225-C.

Steele, M., R. Morley, and W. Ermold (2001), A global ocean hydrography with a high quality Arctic Ocean, *J. Clim.*, *14*, 2079–2087, doi:10.1175/1520-0442(2001)014<2079:PAGOHW>2.0.CO;2.

Stommel, H. (1958), The Abyssal circulation, *Deep Sea Res.*, *5*, 80–82, doi:10.1016/S0146-6291(58)80014-4.

Subrahmanyam, B., V. S. N. Murty, and D. M. Heffner (2011), Sea surface salinity variability in the tropical Indian Ocean, *Remote Sens. Environ.*, *115*, 944–956, doi:10.1016/j.rse.2010.12.004.

Toole, J. M., and B. A. Warren (1993), A hydrographic section across the subtropical South Indian Ocean, *Deep Sea Res., Part I*, *40*, 1973–2019, doi:10.1016/0967-0637(93)90042-2.

Tomczak, M. (1995), Salinity variability in the surface layer of the tropical western Pacific Ocean, *J. Geophys. Res.*, *100*, 20,499–20,515, doi:10.1029/95JC01544.

Valsala, V. K., and M. Ikeda (2007), Pathways and effects of the Indonesian Throughflow water in the Indian Ocean using particle trajectory and tracers in an OGCM, *J. Clim.*, *20*, 2994–3017, doi:10.1175/JCLI4167.1.

van Aken, H. M., H. Ridderinkhof, and W. P. M. de Ruijter (2004), North Atlantic deep water in the south-western Indian Ocean, *Deep Sea Res., Part I*, *51*, 755–776, doi:10.1016/j.dsr.2004.01.008.

Vinayachandran, P. N. (2004), Summer cooling of the Arabian Sea during contrasting monsoons, *Geophys. Res. Lett.*, *31*, L13306, doi:10.1029/2004GL019961.

Vinayachandran, P. N., Y. Masumoto, T. Mikawa, and T. Yamagata (1999), Intrusion of the southwest monsoon current into the Bay of Bengal, *J. Geophys. Res.*, *104*, 11,077–11,085, doi:10.1029/1999JC900035.

Webster, P. J., V. O. Magaña, T. N. Palmer, J. Shukla, R. A. Tomas, M. Yanai, and T. Yasunari (1998), Monsoons: Processes, predictability, and the prospects for prediction, *J. Geophys. Res.*, *103*(C7), 14,451–14,510, doi:10.1029/97JC02719.

Webster, P. J., A. M. Moore, J. P. Loschnigg, and R. R. Leben (1999), Coupled ocean-atmosphere dynamics in the Indian Ocean during 1997-98, *Nature*, *401*, 356–360, doi:10.1038/43848.

Wijffels, S. E., R. W. Schmitt, H. L. Bryden, and A. Stigebrandt (1992), Transport of freshwater by the oceans, *J. Phys. Oceanogr.*, *22*, 155–162, doi:10.1175/1520-0485(1992)022<0155:TOFBTO>2.0.CO;2.

E. S. Nyadjro and B. Subrahmanyam, Marine Science Program, University of South Carolina, Columbia, SC 29205, USA. (enyadjro@geol.sc.edu)

J. F. Shriver, Naval Research Laboratory, Stennis Space Center, MS 39529, USA.